

Research Article

Implementation of a Transform-Minutiae Fusion-Based Model for Fingerprint Recognition

Justice Kwame Appati , Prince Kofi Nartey , Ebenezer Owusu ,
and Ismail Wafaa Denwar 

Department of Computer Science, University of Ghana, Accra, Ghana

Correspondence should be addressed to Ebenezer Owusu; ebeowusu@ug.edu.gh

Received 27 January 2021; Revised 13 February 2021; Accepted 19 February 2021; Published 4 March 2021

Academic Editor: Chin-Chia Wu

Copyright © 2021 Justice Kwame Appati et al. This is an open access article distributed under the Creative Commons Attribution License, which permits unrestricted use, distribution, and reproduction in any medium, provided the original work is properly cited.

Biometrics consists of scientific methods of using a person's unique physiological or behavioral traits for electronic identification and verification. The traits for biometric identification are fingerprint, voice, face, and palm print recognition. However, this study considers fingerprint recognition for in-person identification since they are distinctive, reliable, and relatively easy to acquire. Despite the many works done, the problem of accuracy still persists which perhaps can be attributed to the varying characteristic of the acquisition devices. This study seeks to improve the issue recognition accuracy with the proposal of the fusion of a two transform and minutiae models. In this study, a transform-minutiae fusion-based model for fingerprint recognition is proposed. The first transform technique, thus wave atom transform, was used for data smoothing while the second transform, thus wavelet, was used for feature extraction. These features were added to the minutiae features for person recognition. Evaluating the proposed design on the FVC 2002 dataset showed a relatively better performance compared to existing methods with an accuracy measure of 100% as to 96.67% and 98.55% of the existing methods.

1. Introduction

Biometrics deals with the technology used for electronic identification and verification of an individual based on behavioral and physiological characteristics they possess [1]. It focuses on scientific approaches for identifying these individuals uniquely based on these characteristics. These traits are known to be unique for every person. Some standard biometric identification methods are fingerprint recognition, voice recognition, facial recognition, and signature dynamics. Biometric devices are conventionally made of a biometric engine. A biometric engine is a program that operates together with the biometric systems' hardware devices. Its purpose is to administer biometric data during the capture, extraction, and matching process stages [2]. Successful research into biometric technologies has significantly improved the reliability and security of identification, authentication, and verification standards [3].

There are several other biometric authentication techniques. However, this research adopts the fingerprint recognition technique as its area of discussion. The reason for this choice is that fingerprints have recently been adopted extensively and successfully to aid in proof of identity because of their originality, durability through history, peculiarity, public acceptance, and the minimal risk of personal invasion that characterize fingerprint matching [4]. A fingerprint is the impression of patterns from a finger's surface [5]. Because fingerprint-based authentication and identification are distinct for every person and are not significantly distorted with age, it is one of the most common biometric technologies. Aside from being relatively inexpensive to implement, the main reasons why fingerprint recognition has become the most widely used biometric authentication approach, averaging more than 50 percent of all recognition systems currently in use, are factors such as the distinctiveness, reliability, and relative ease of acquisition [6]. Due to its numerous

advantages, a considerable number of researchers' attention has been drawn to the fingerprint identification method in recent years [4]. One of the main benefits is that the legal community acknowledges its use for personal identification. This identification technique is effortless, accurate, cheap, and relatively easy to identify [7].

Moreover, this recognition approach is widely recognized for its authentication precision and the likelihood that the same fingerprint occurring in two persons is minimal. All said and done, there are other instances where the system fails to recognize some fingerprints due to the possibility that the fingerprint reader may lose its sensitivity with time, or a user's fingerprint might be damaged [8]. These problems lend us to two main errors in recognition, thus Type-I and Type-II errors. When a recognition system rejects an authorized user, a Type-I error or false rejection is expected. In contrast, the system may accept imposters, leading to an unauthorized access granted resulting in a Type-II error or the occurrence of false acceptance [4]. These errors are the motivations to building a system that properly mitigates against these two types of errors. Fingerprint distinctiveness can be attained by analyzing minutiae points, ridge, and furrow patterns. Identifying minutiae and patterns are imperative for recognizing fingerprints because no two fingerprints are the same [9].

Extensive research works on fingerprint recognition systems have been carried out, and several approaches and techniques have been proposed, yet the issue of recognition accuracy still exists in fingerprint recognition [4]. Further research is still ongoing to resolve the accuracy problem, mostly due to mismatch or misclassification of extracted fingerprint features. Therefore, the features to be extracted for recognition must be acceptable to improve accuracy. The subsequent sections of the paper are organized as follows. The methodology is introduced in Section 2. Section 3 discusses experimentation. Section 4 extensively discusses the results recorded. Lastly, the work is concluded in Section 5.

2. Research Design

This section discusses the fingerprint image preprocessing and how these fingerprint characteristics are extracted to aid in person recognition.

2.1. Fingerprint Image Preprocessing. The preprocessing of the fingerprint images is imperative in building a successful recognition or authentication system. This section discusses the various stages of smoothing fingerprint images to help extract relevant features for accurate recognition. The wave atom denoising technique was leveraged on for this study for image smoothing. Image normalization, ridge orientation, and estimation are further performed as outlining the subsequent subsections.

2.1.1. Wave Atom Transform Technique for Smoothing. In numerical analysis and processing of images, a wave atom transform is a new technique used for performing multiscale transforms proposed by Demanet and Ying [10], as shown in

Figure 1. The technique is known to accurately demonstrate both multiscale and multidirectional properties, given an image data [4]. For a better appreciation of this transform compared with other transforms, two indexes α and β are introduced in the analysis of its scheme [11]. The parameter α denotes a multiscale decomposition while β defines the localization of basic elements. From the figure shown, the parametric value satisfying a wavelet transform is $\alpha = \beta = 1$, the Gabor transform is $\alpha = \beta = 0$, curvelets are $\alpha = 1$ and $\beta = 1/2$, and ridgelets are $\alpha = 1$ and $\beta = 0$. However, the wave atom transform demonstrates a trade-off between multiscale and multidirectional spaces with $\alpha = \beta = 1/2$ making it a choice that might be useful in this study as a denoising technique.

2.1.2. Image Normalization. The normalization of the fingerprint images was necessary in this study to adjust the intensity of the values [12]. Mathematically, the normalization is a linear pixel-wise operator which helps lessen the gray-level variations along the furrows and ridges which are features of interest while achieving an invariant mean and variance. Besides, the dataset for the study was captured with varying finger pressures and sensor noise effects to exhibit a real industrial scenario and these effects require normalization to reduce their prevalence. In its implementation, a window of size $w \times w$ is used to enhance the computational time. Given an image $\text{img}(i, j)$, with an estimated Mean M_i and Variance V_i , the normalized image $N(i, j)$ can be defined as

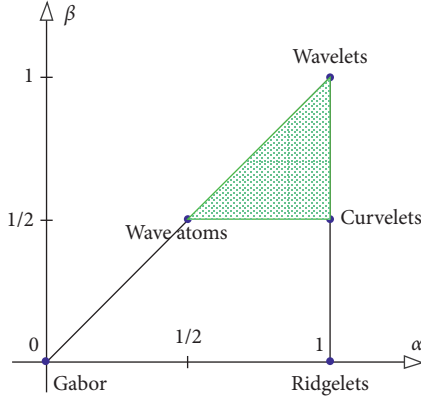
$$N(i, j) = \begin{cases} M_0 + \sqrt{V_0 (\text{img}(i, j) - M_i)^2}, & \text{if } \text{img}(i, j) > M, \\ M_0 - \sqrt{V_0 (\text{img}(i, j) - M_i)^2}, & \text{otherwise.} \end{cases} \quad (1)$$

Once the fingerprint image is normalized, the orientation of the ridges and furrows are estimated as outlined in Section 2.1.3.

2.1.3. Ridge Orientation Estimation. In order to detect points of singularity from a given fingerprint image, ridge orientations are estimated [13]. The ridges and furrows possess unique patterns of flow exhibiting several orientations that ranges from 0 to 180 degrees denoted by $\theta(i, j)$. Instead of defining a single pixel, the image map is localized with a block operator as outlined as follows:

- (a) The input image is divided into nonoverlapping $w \times w$ block sizes.
- (b) The image gradients δx and δy for each pixel in the block are computed. This image gradient map can be estimated using operators such as Canny and Sobel and among others. Equation (2) is an example of the Sobel gradient operator:

$$G_x = \begin{bmatrix} -1 & 0 & 1 \\ -2 & 0 & 2 \\ -1 & 0 & 0 \end{bmatrix} \text{ and } G_y = \begin{bmatrix} -1 & 2 & -1 \\ 0 & 0 & 0 \\ 1 & 2 & 1 \end{bmatrix}. \quad (2)$$

FIGURE 1: Various transforms (α, β) as wave packet families [10].

(c) The computation of the local field orientation is then estimated using

$$V_x = \sum_{u=i-(w/2)}^{i+(w/2)} \sum_{v=i-(w/2)}^{i+(w/2)} 2\delta_x(u, v)\delta_y(u, v), \quad (3)$$

$$V_y = \sum_{u=i-(w/2)}^{i+(w/2)} \sum_{v=i-(w/2)}^{i+(w/2)} \delta_x^2(u, v)\delta_y^2(u, v). \quad (4)$$

From these two equations, the orientation field is estimated with

$$\theta(i, j) = \frac{1}{2} \frac{V_y(i, j)}{V_x(i, j)}. \quad (5)$$

(d) At this point, it is expected that some level of noise will be introduced leading a point of discontinuity in the orientation field. This effect could be minimized or softened using a low-pass filter; however, this process requires that the orientation field be transformed into a continuous vector field as shown in the following equations:

$$\mathcal{O}_x(i, j) = \cos \cos(2\theta(i, j)), \quad (6)$$

$$\mathcal{O}_y(i, j) = \sin \sin(2\theta(i, j)). \quad (7)$$

(e) The low-pass filter can then be applied to the resultant output of equations (6) and (7) as expressed in

$$\mathcal{O}'_x = \sum_{u=-(h/2)}^{(h/2)} \sum_{v=-(h/2)}^{(h/2)} G(u, v) \cdot \mathcal{O}_x(i - uw, j - vw), \quad (8)$$

$$\mathcal{O}'_y = \sum_{u=-(h/2)}^{(h/2)} \sum_{v=-(h/2)}^{(h/2)} G(u, v) \cdot \mathcal{O}_y(i - uw, j - vw). \quad (9)$$

(f) Finally, the smoothed orientation field can be obtained with

$$\theta(i, j) = \frac{1}{2} \tan^{-1} \frac{\theta'_y(i, j)}{\theta'_x(i, j)}. \quad (10)$$

This orientation field is now used to identify the fingerprint core point which is a keypoint feature.

2.2. Feature Extraction. This section describes in detail the characteristics of fingerprints and how they are extracted for person identification. Broadly features of a fingerprint image can be grouped into two: global and local. The global fingerprint features include delta and core points also known as singular points, as well as the ridge orientation and spacing [14].

2.2.1. Fingerprint Characterization. According to Maltoni et al. [15] in their book “Handbook of Fingerprint Recognition,” there are three basic fingerprint ridge patterns: the arch, loop, and whorl.

The Arch. With this pattern, as depicted in Figure 2, the finger’s ridges emerge from one edge, curve up in the midsection forming an arc, and then end on the opposite edge without rotating centrally. The arch pattern can be classified into four main types [4], that is, plain, radial, ulnar, and tented arch.

The Loop. With this pattern, as shown in Figure 3, the ridges emerge from one edge of the finger, make a curve, and then end back at the same edge where the ridges initially emerged. Loops are classified into four types [4]: plain, central pocket, lateral pocket, and twinned loop patterns.

The Whorl. With this pattern, as shown in Figure 4, ridges are circularly formed in the finger’s midsection. Delta point formations in these patterns classify them into four types [4]: accidental whorl, double-pocket loop whorl, central pocket loop whorl, and plain whorl patterns.

2.2.2. Fingerprint Keypoints. On the other hand, minutiae points are local characteristics on a fingerprint that exist either as a ridge ending or a bifurcation [1]. In brief, the ridge ending is the termination point of ridges on the fingerprint while a ridge bifurcation is a point on the fingerprint where one ridge splits into two different ridges. In general, the minutiae characteristics of fingerprint as enlisted in The Guardia Civil Database (GCDB) in Spain, is as shown in Figure 5.

Labels of the minutiae characteristics in Figure 5 are tabulated in Table 1.

2.2.3. Minutiae Extraction with Sequential Binarization. In theory, a sequential approach to binarization is easy and effective for extraction of features from the point of view of design and processing. In general, the following three steps consist of a sequential binarization procedure: binarization, thinning, and minutiae extraction [16].

Binarization. The original grayscale image is converted into a binary image which presents the image as a 2D gray-level intensity function $f(x, y)$ with values ranging from 0 to $L - 1$, where L denotes all individual gray-levels. Let n denote the total number of pixels in an image and n_i be the number of pixels with gray-level i , and the probability that gray-level i may occur is defined as



FIGURE 2: The arch.



FIGURE 3: The loop.



FIGURE 4: The whorl.

$$p_i = \frac{n_i}{n}. \quad (11)$$

The fingerprint image gray-level is averaged with

$$\mu_T = \sum_{i=0}^{L-1} i p_i. \quad (12)$$

After averaging, the fingerprint image pixels are classified into two distinct groups: $C_1 = \{0, 1, \dots, t\}$ and $C_2 = \{t + 1, t + 2, \dots, L - 1\}$ with t as the threshold value. The objects of interest in the foreground and background of a given image correspond to the C_1 and C_2 , respectively. Equations (13) and (14) are the respective probabilities:

$$\omega_1(t) = \sum_{i=0}^t p_i, \quad (13)$$

$$\text{and } \omega_2(t) = \sum_{i=t+1}^{L-1} p_i. \quad (14)$$

The average gray-level values for C_1 and C_2 are calculated, respectively, with the following equations:

$$\mu_1(t) = \sum_{i=0}^t \frac{i p_i}{\omega_1(t)}, \quad (15)$$

$$\text{and } \mu_2(t) = \sum_{i=t+1}^{L-1} \frac{i p_i}{\omega_2(t)}. \quad (16)$$

Thinning. After the binarization process is complete, the thinning process is engaged to reduce the ridge line thickness to one pixel. This operation is imperative to allow for simplification of the resultant image for accurate extraction of features. The thinning process firstly divides the image into two separate maps in a checkered arrangement. In the initial subiteration, pixel p is deleted from the first image map if the G_1 , G_2 , and G_3 conditions are met while pixel p is deleted from the second image map if the G_1 , G_2 , and G_4 conditions are all met in the final subiteration. The condition is defined as follows.

Condition G_1 is presented in equation (17) with its variables defined in equation (18):

$$X_H(p) = 1, \quad (17)$$

where

$$X_H(p) = \sum_{i=1}^4 b_i, \\ b_i = \begin{cases} 1, & \text{if } x_{2i-1} = 0 \text{ and } x_{2i} = 1 \text{ or } x_{2i+1} = 1, \\ 0, & \text{otherwise.} \end{cases} \quad (18)$$

The values x_1, x_2, \dots, x_8 are the 8 neighbors of p , beginning with the east neighbors and counted in an anti-clockwise manner.

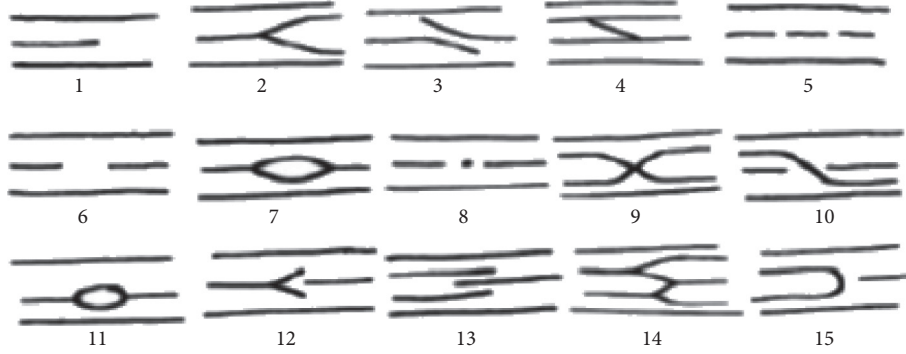


FIGURE 5: The Guardia Civil database minutiae characteristics [7].

TABLE 1: Labeling of minutiae characteristics.

No.	Name
1	Ridge ending
2	Bifurcation
3	Deviation
4	Bridge
5	Fragment
6	Interruption
7	Enclosure
8	Point
9	Ridge crossing
10	Transversal
11	Circle
12	Delta
13	Assemble
14	M-structure
15	Return

Condition G_2 is shown in equation (19) as

$$2 \leq \min\{n_1(p), n_2(p)\} \leq 3, \quad (19)$$

where

$$n_1(p) = \sum_{k=1}^4 x_{2k-1} \vee x_{2k}, \quad (20)$$

$$n_2(p) = \sum_{k=1}^4 x_{2k} \wedge x_{2k+1}. \quad (21)$$

Condition G_3 is shown in equation (22) as

$$(x_2 \vee x_3 \vee \bar{x}_8) \wedge x_1 = 0. \quad (22)$$

Condition G_4 is shown in equation (23) as

$$(x_6 \vee x_7 \vee \bar{x}_4) \wedge x_5 = 0. \quad (23)$$

At the end of the thinning process, some pixels considered as spur pixel, h -connected pixel, and isolated pixels emerge, which are cleaned up. Finally, a bridge operator is applied to the resultant image to maintain an optimal skeleton appropriate for minutiae extraction.

Minutiae Extraction. This process involves determining whether or not pixels belong to distinct ridges and, in which case, whether the ridges are ending points or bifurcations, thereby acquiring a candidate minutiae group. The x and y coordinates are recorded for every detected minutia as well as the orientation and the corresponding ridge feature. The extraction of minutiae is performed using the crossing number method which is one of the most popular techniques for this kind of task [17]. The method uses a 3×3 window to check the local neighborhoods of each ridge pixel p in the image. By definition, the crossing number of p is half the sum of the differences between adjacent pixel pairs that form the 8-neighborhood of p , as given in

$$CN = 0.5 \sum_{i=1}^8 |P_i - P_{i+1}|, \quad (24)$$

where P_i denotes the pixel's value (one or zero) in a 3×3 neighborhood of P , as shown in Figure 6.

The crossing number and its corresponding characteristic are listed in Table 2.

In summary, the following is the algorithm for finding minutiae:

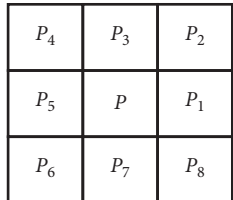
- Input: fingerprint image
- Output: ridge endings and bifurcations
- Step 1: binarize input fingerprint image.
- Step 2: apply thinning to the image.
- Step 3: analyze the thinned fingerprint image and detect the minutiae by using the 8-neighborhood pixels to compute for each block of the ridge bifurcations and ridge endings.
- Step 4: store the detected minutiae in a file.
- Step 5: end.

Once the minutiae point coefficients are extracted, the wavelet coefficient extraction process is performed next.

2.2.4. Wavelet Transform Technique. In computing the wavelet transform (DWT) for the fingerprint images, low-pass and high-pass filters are used to convolve the smoothed images. A downsampling procedure is applied by columns on the images obtained. Here, all indexed columns are

TABLE 2: Crossing number characteristics.

CN	Characteristics
0	Isolated point
1	End point
2	Continuing point
3	Bifurcation point
4	Crossing point

FIGURE 6: A 3×3 mask.

chosen, after which high-pass and low-pass filters are used to convolve the images again with rows downsampling procedure. Consequentially, four subband images of half the size of original images are obtained. These generated subband images hold the approximation (A), vertical (V), horizontal (H), and diagonal (D) information of the fingerprint image. Amongst the four subband images, the approximation coefficients hold significant information of the fingerprint image. Due to this, it is a primary choice for our feature selection. The Daubechies 9 (db9) wavelet is considered in this study as it generates similar results compared to complex Gabor wavelets [18]. It also extracts more appropriate features from an image relative to simpler wavelets such as Haar. Finally, it takes less time to retrieve results than other complex wavelet techniques [19]. A general expression for the wavelet transform is shown in

$$F(a, b) = \int_{-\infty}^{\infty} f(x)\psi_{(a,b)}^*(x)dx, \quad (25)$$

where* represents the complex conjugate while the function ψ is any function satisfying some well-defined properties [20]. Several types of wavelets exist and can be classified based on the orthogonality property. This property helps develop the discrete wavelet transform while the continuous wavelet transforms can be generated using the non-orthogonal wavelets. The two transform types are characterized by the following properties [20]:

- (1) With discrete wavelet transforms, a data vector of the same size as the input is returned. Typically, a large number of data in this vector are almost zero. The main reason is that the input signal is decomposed into a group of functions or wavelets equilateral to its scaling and translations. Hence, this signal decomposition returns an equal or lower number of the wavelet coefficient spectrum as the number of signal data points.
- (2) However, continuous wavelet transforms return arrays that are a single dimension larger than their input data.

The db9 wavelet transform is applied to the fingerprint images to extract these coefficients for the recognition of the fingerprint. Once both minutiae and db9 wavelet coefficients are extracted for each image, the corresponding features are merged with concatenation operator to form a single matrix. The resultant matrix is partitioned into the training and testing dataset using 75 : 25 criteria.

2.3. Classification Techniques

2.3.1. Support Vector Machine (SVM). This study looks at a multiclass classification problem and used a multiclass SVM for this purpose. The classifier utilizes $K(K - 1)/2$ binary SVM models using the one-versus-one coding design, with K being the number of different class labels. The SVM algorithm is mainly used for locating a hyperplane that precisely groups the associated feature points into classes in an N -dimensional space with N features [21]. Sets of data points that occur on either side of a hyperplane can be banded together into separate classes. However, the number of features available determines the dimension of the hyperplane. For instance, if there are 2 input features, the dimension of the hyperplane produced becomes a line as depicted in Figure 7. If input features are 3, then a two-dimensional hyperplane will be produced as depicted in Figure 8. Therefore, it becomes quite challenging to determine when the number of features goes beyond the value of 3.

To distinguish between the two data point classes, there are several possible choices of hyperplanes to be selected. The objective is to determine a plane with the largest margin, such as the most significant distance between each class's data points. The margin distance is maximized to provide some room to classify future data points with more surety. The feature points closest to the hyperplane that affects its direction and location are called support vectors. With the support vectors obtained, the classifier margin is maximized, as shown in Figure 9.

2.4. Performance Evaluation. This study's main objective is to improve fingerprint recognition accuracy, such as other biometric authentication systems; in this proposed model, an input fingerprint image is compared to the database templates. A classification process helps to accept or reject the user. To achieve this, the metrics used to measure this model's performance are precision, recall, and recognition accuracy, as stated in equations (26) to (28), respectively. The precision defines what numbers of positive predictions were positive. Recall on the other hand defines the number of all positive samples that were correctly predicted as positive by the classifier. Recall can also be referred to as true positive rate (TPR). From the equations listed, TP denotes true positive, FP denotes false positive, and FN denotes false negative:

$$\text{accuracy} = \frac{\text{TP} + \text{FN}}{\text{TP} + \text{FP} + \text{TN} + \text{FN}}, \quad (26)$$

$$\text{precision} = \frac{\text{TP}}{\text{TP} + \text{FP}}, \quad (27)$$

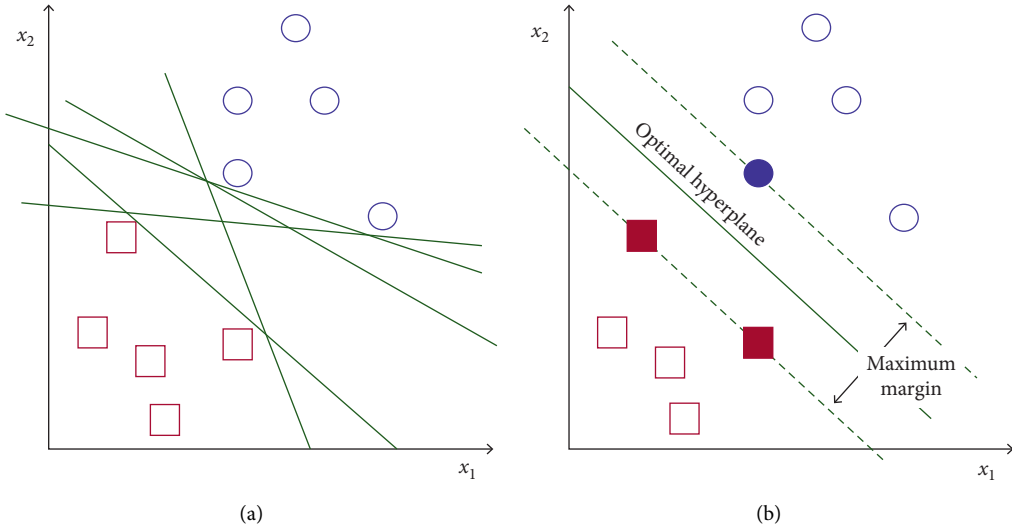


FIGURE 7: Possible hyperplanes (left) and optimal hyperplane (right).

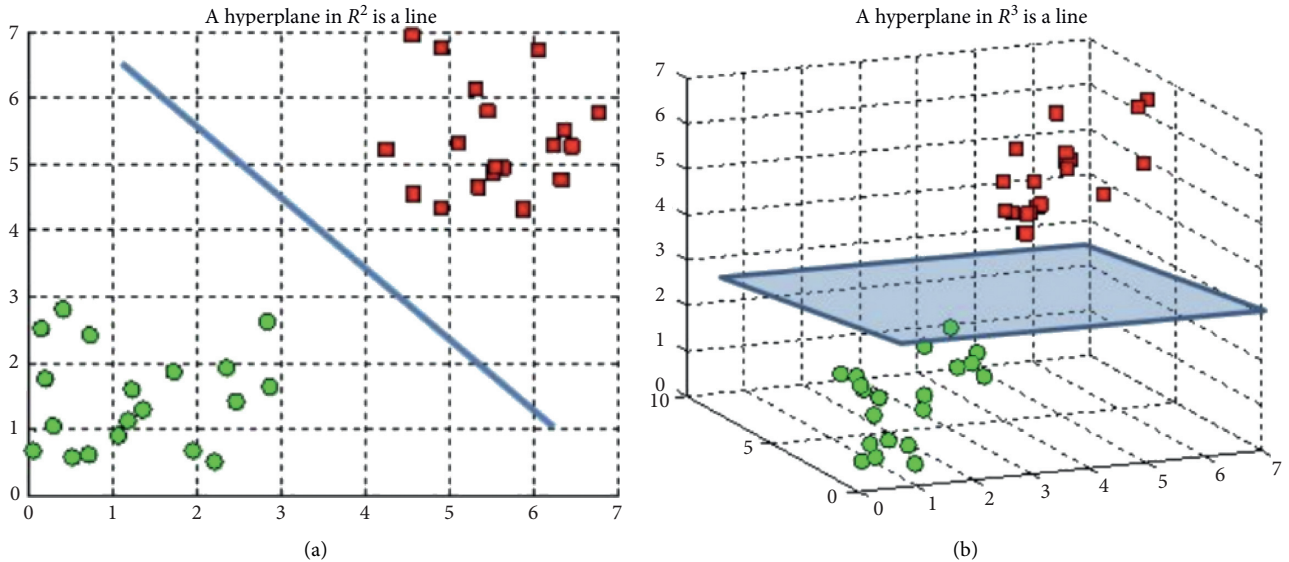


FIGURE 8: Hyperplanes in 2D (left) and 3D (right).

$$\text{recall} = \frac{\text{TP}}{\text{TP} + \text{TN}}. \quad (28)$$

3. Results and Discussion

This section of the study reports data acquisition, information, and analysis of the acquired fingerprint dataset. The computational experience and results obtained from the evaluation are comparatively discussed.

3.1. Dataset Availability and Information. The National Institute of Standards and Technology (NIST), the Fingerprint Verification Competition (FVC), and the Hong Kong Polytechnic University High-Resolution Fingerprint

(PolyU HRF), among others, are databases available online for evaluation purposes upon request. For a fair comparison with existing studies, this study uses the FVC2002 for its model evaluation. The selected dataset generally comes in four forms thus as follows: DB1, DB2, DB3, and DB4. Each dataset has 880 grayscale fingerprints in all, made up of 110 fingers with 8 impressions each. Each dataset is divided into two sets, A and B with the following naming convention: DB1_A and DB1_B, DB2_A and DB2_B, in that order. Set A contains fingerprints labeled 1 to 100 (800 impressions in total), and Set B contains those labeled 101 to 110 (80 impressions in total) for each. This study used all the FVC2002 Set B (DB1_B, DB2_B, DB3_B, and DB4_B) images resulting in 320 impressions in total for evaluation. The DB1_B images were obtained from an optical sensor, "TouchView II" by Identix, which gave an image size of

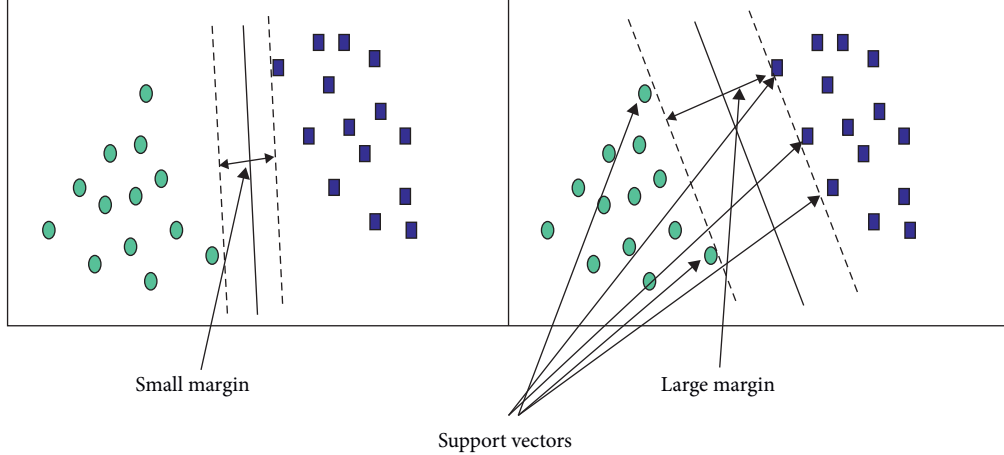


FIGURE 9: Support vectors.

388×374 (142 Kpixels) with 500 dpi each. Likewise, the DB2_B images were obtained from an optical sensor “FX2000” by Biometrika, which also gave an image size of 296×560 (162 Kpixels) with 569 dpi each. The DB3_B images were captured with a capacitive sensor “100 SC” by Precise Biometrics, and image sizes are 300×300 (88 Kpixels) with 500 dpi each. Finally, the DB4_B images were obtained from a synthetic fingerprint generator, “SFinGe v2.51,” which had an image size of 288×384 (108 Kpixels) with about 500 dpi each. All these variations introduce some level of difficulty when it comes to their analysis. Figure 10 depicts the 8 fingerprint impressions from the finger of individual 101 in the DB1_B database.

3.2. Analysis of Results of Proposed Approach. As an overview of the proposed method, the wave atom denoising is performed on all fingerprint images of the selected dataset, from which both wavelet coefficients and minutiae are extracted and saved. The extracted minutiae and wavelet coefficients are concatenated to form a single feature matrix for the purpose of classification. Pictorially, Figure 11 gives the schematic view of the proposed pipeline.

3.2.1. Fingerprint Denoising. Each grayscale fingerprint image is denoised and smoothed using wave atom transform. Firstly, a right circular shift process is applied to the input fingerprint image, after which the forward 2D wave atom transform is applied. The resultant output of the process is the wave atom coefficients. Hard thresholding is applied to these coefficients to remove noisy signals and the inverse 2D wave atom transform is then applied afterward. Lastly, a left circular shift is applied to the output to complete the image denoising process. The denoised fingerprint image is then reorganized from the final set of coefficients as shown in Figure 12.

3.2.2. Discrete Wavelet Transform Coefficients. Each denoised fingerprint image is decomposed into the four subbands resulting in Figure 13.

This operation is repeated four times successively on the approximation coefficient. At the fourth level of the decomposition process, a set of forty-seven Daubechies 9 coefficient was extracted. These coefficients which represent the characteristic features of a given fingerprint are extracted from the approximation subbands. The resultant features are appended to the extracted minutiae in Section 3.2.3.

3.2.3. Minutiae Extraction. The core point, ridge endings, and bifurcations on the fingerprints were detected, while removing spurious minutiae. This is done by binarizing the fingerprint image, thinning the binarized image, and detecting the minutiae. The input image and its corresponding binarized image are shown in Figure 14.

In Figure 15, we have the thinned image (left) created from the binarized image and an overlay of the minutiae (right) on the thinned image after removing all spurious minutiae. The red spots represent ridge endings, the pink and blue spots represent bifurcations, and the green spot represents the core point.

The numeric features of the corresponding minutiae points for each fingerprint are extracted and stored. A sample feature vector representing the first three impressions of finger 101 is shown in Table 3.

3.2.4. Numerical Evaluation of Proposed Approach. The metrics precision, recall, and recognition accuracy are computed separately for all four datasets evaluated using the proposed approach. Evaluation of the four FVC2002 Set B datasets was performed separately mainly for comparison with previous works. A summary of the results from the experimentation is shown in Table 4. Moreover, Table 5 shows the model’s performance on each of the two features when experimented separately.

3.3. Comparative Analysis. The proposed method is compared with previous works from other studies that experimented on the same datasets used for evaluation, thus the FVC2002 DB1_B dataset.



FIGURE 10: The 8 impressions from finger 101.

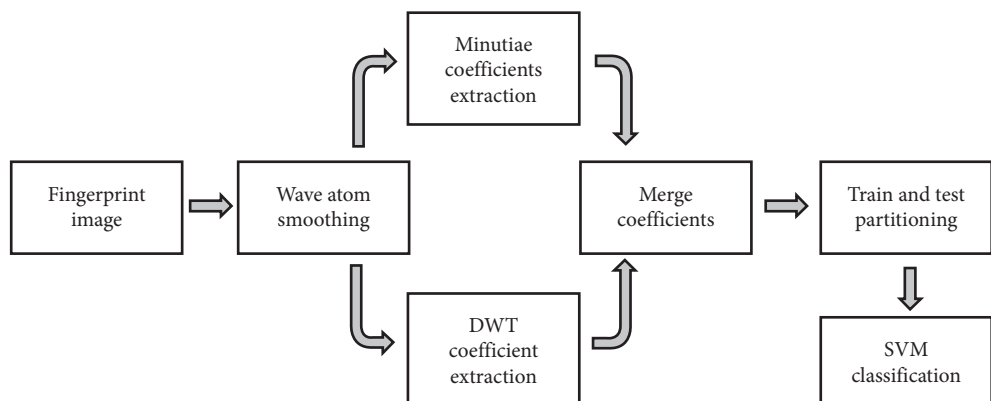


FIGURE 11: Design pipeline.



FIGURE 12: Input image (left) and smoothed image using wave atom transform (right).

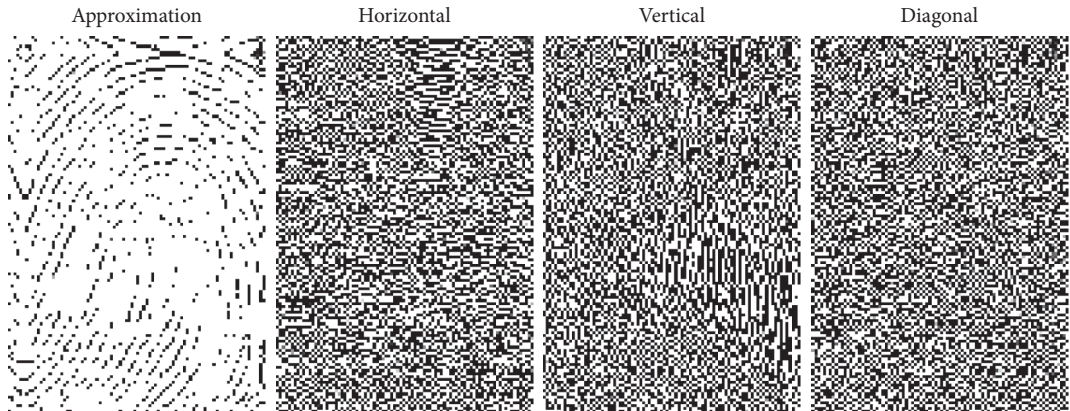


FIGURE 13: Details of DWT fingerprint image decomposition.



FIGURE 14: Input fingerprint image (left) and binarized image (right).



FIGURE 15: Thinned image (left) and display of minutiae (right).

TABLE 3: Feature vector representation of the first three impressions of fingers 101.

Finger ID	x coordinate	y coordinate	Crossing number	Angle
101_1.tif	90.4696	120.3922	1.729448	1.978024
101_2.tif	120.80335	108.6511	2.059126	1.979613
101_3.tif	101.3366	104.6962	1.973153	1.884723

TABLE 4: Performance of various datasets.

Dataset	Precision	Recall	Recognition accuracy (%)
DB1_B (TouchView II optical sensor)	1.00	1.00	100
DB2_B (FX2000 optical sensor)	0.95	0.95	95
DB3_B (100 SC capacitive sensor)	1.00	1.00	100
DB4_B (SFinGe v2.51 synthetic FP generator)	0.95	0.95	95

TABLE 5: Performance of separate features (minutiae and DWT).

Dataset	Minutiae only (%)	DWT only (%)
DB1_B (TouchView II optical sensor)	50	95
DB2_B (FX2000 optical sensor)	70	80
DB3_B (100 SC capacitive sensor)	40	95
DB4_B (SFinGe v2.51 synthetic FP generator)	65	40

TABLE 6: A comparative analysis of experimental results using the FVC 2002 DB1_B dataset.

Method by	Database	Features	Recognition accuracy (%)
Sang et al. [22]	DB1_B	Minutiae + invariant moment	96.67
Ali et al. [23]	DB1_B	Minutiae	98.55
Proposed approach	DB1_B	Minutiae + db9 wavelet	100.00

As observed in Table 6, this study's proposed approach performs considerably better than the named authors' previous works. The proposed model in general performs significantly well when tested on the other three datasets of FVC2002-DB2_B, DB3_B, and DB4_B with a recognition accuracy of 95%, 100%, and 95%, respectively.

4. Discussion

It is observed from Table 4 that each of the four datasets was obtained from different sensors. However, the proposed model performed relatively well, with 100% accuracy for DB1_B and DB3_B. On the contrary, the model wrongly predicted one out of 20 test data in the other two datasets, which yielded 95% accuracy. However, upon further experimentation on the extracted features as disjoint sets to ascertain the proposed model's performance, DWT features yielded a near accurate score of 95% on DB1_B. Nonetheless, on testing the model on minutiae features only, a prediction accuracy of 50% was recorded which is considerably poor. The results from DB2_B also show relatively good prediction accuracies of 80% and 70% for DWT features and minutiae features, respectively. For DB3_B, the model's performance was poor with the minutiae features with an accuracy score of 40% but performed better on the DWT features yielding 95% accuracy. The performance for DB4_B in contrast to the initial datasets yielded a higher percentage accuracy for the minutiae features, with 65% compared to a relatively low accuracy of 40% for the DWT

features. From the experimentation, it was realized that the prediction accuracy rises significantly when more features (columns) are added during the feature selection stage of the model; hence, the smaller the number of features selected, the lower the prediction accuracy. This may account for the lower scores produced for the minutiae features, which are only 6 for each finger impression, compared to 47 features for DWT producing better results.

5. Conclusion

This study proposed and presented a transform-minutiae fusion-based model to improve the accuracy of fingerprint recognition. The wave atom denoising approach was proposed to initially remove noise from fingerprint images for better feature detection and extraction. In the proposed method, both minutiae and wavelet transform coefficients (db9 wavelet) are extracted and used for recognition. The datasets used for evaluation were from all the FVC 2002 Set B databases (DB1_B, DB2_B, DB3_B, and DB4_B) consisting of 320 fingerprint images in total. The proposed method proved to perform better with a recognition accuracy of 100% as compared with previous studies using the DB2_B dataset.

Data Availability

The data employed to support this study's experimentation can be obtained from FVC2002 (<http://bias.csr.unibo.it/fvc2002/>).

Conflicts of Interest

The authors declare that there are no conflicts of interest regarding the publication of this paper.

References

- [1] J. Galbally, R. Haraksim, and L. Beslay, "A study of age and ageing in fingerprint biometrics," *IEEE Transactions on Information Forensics and Security*, vol. 14, no. 5, pp. 1351–1365, 2019.
- [2] T. Sabhanayagam, V. Prasanna Venkatesan, and K. Senthamarikannan, "A comprehensive survey on various biometric systems," *International Journal of Applied Engineering Research ISSN*, vol. 13, no. 5, pp. 2276–2297, 2018, <http://www.ripublication.com>.
- [3] S. Gu, J. Feng, J. Lu, J. Zhou, and S. Member, "Efficient rectification of distorted fingerprints," *IEEE Transactions on Information Forensics and Security*, vol. 13, no. 1, pp. 156–169, 2018.
- [4] S. R. Borra, G. J. Reddy, and E. S. Reddy, "A broad survey on fingerprint recognition systems," in *Proceedings of the 2016 IEEE International Conference on Wireless Communications, Signal Processing and Networking, WiSPNET*, pp. 1428–1434, Chennai, India, March 2016.
- [5] K. Cao and A. K. Jain, "Learning fingerprint reconstruction: from minutiae to image," *IEEE Transactions on Information Forensics and Security*, vol. 10, no. 1, pp. 104–117, 2015.
- [6] K. Abhishek and A. Yogi, "A minutiae count based method for fake fingerprint detection," *Procedia Computer Science*, vol. 58, pp. 447–452, 2015.
- [7] R. P. Krish, J. Fierrez, D. Ramos, F. Alonso-Fernandez, and J. Bigun, "Improving automated latent fingerprint identification using extended minutia types," *Information Fusion*, vol. 50, pp. 9–19, 2019.
- [8] P. Tertychnyi, C. Ozcinar, and G. Anbarjafari, "Low-quality fingerprint classification using deep neural network," *IET Biometrics*, vol. 7, no. 2, pp. 550–556, 2018.
- [9] W. Yang, S. Wang, J. Hu, G. Zheng, and C. Valli, "Security and accuracy of fingerprint-based biometrics: a review," *Symmetry*, vol. 11, no. 2, p. 141, 2019.
- [10] L. Demanet and L. Ying, "Wave atoms and sparsity of oscillatory patterns," *Applied and Computational Harmonic Analysis*, vol. 23, no. 3, pp. 368–387, 2007.
- [11] Z. Haddad, A. Beghdadi, A. Serir, and A. Mokraoui, "Wave atoms based compression method for fingerprint images," *Pattern Recognition*, vol. 46, no. 9, pp. 2450–2464, 2013.
- [12] A. Arif, T. Li, and C. H. Cheng, "Blurred fingerprint image enhancement: algorithm analysis and performance evaluation," *Signal, Image and Video Processing*, vol. 12, no. 9, pp. 767–774, 2017.
- [13] K. N. Win, K. Li, J. Chen, and P. F. Viger, "Fingerprint classification and identification algorithms for criminal investigation: a survey," *Future Generation Computer Systems*, vol. 110, pp. 758–771, 2019.
- [14] M. Liu, S. Liu, and W. Yan, "Latent fingerprint segmentation based on ridge density and orientation consistency," *Security and Communication Networks*, vol. 2018, Article ID 4529652, 10 pages, 2018.
- [15] D. Maltoni, D. Maio, A. K. Jain, and S. Prabhakar, *Handbook of Fingerprint Recognition*, Springer-Verlag, New York, NY, USA, 2009.
- [16] P. Amoako-Yirenkyi, N. Frempong, J. Appati, J. Hafron-Acquah, and I. Dontwi, "Threshold analysis of wavelet based fingerprint feature extraction methods on multiple impression dataset," *British Journal of Mathematics & Computer Science*, vol. 5, no. 3, pp. 383–396, 2015.
- [17] S. Shi, J. Cui, X.-L. Zhang, Y. Liu, J.-L. Gao, and Y.-J. Wang, "Fingerprint recognition strategies based on a fuzzy commitment for cloud-assisted IoT: a minutiae-based sector coding approach," *IEEE Access*, vol. 7, pp. 44803–44812, 2019.
- [18] A.-C. Phan, H.-D. Tran, and T.-C. Phan, "Fingerprint recognition using gabor wavelet in MapReduce and spark," in *Proceedings of the Ninth International Symposium on Information and Communication Technology: SoICT 2018*, pp. 54–60, Danang City Vietnam, December 2018.
- [19] V. Srivastava and R. K. Purwar, "A five-level wavelet decomposition and dimensional reduction approach for feature extraction and classification of MR and CT scan images," *Applied Computational Intelligence and Soft Computing*, vol. 2017, Article ID 9571262, 9 pages, 2017.
- [20] E. Khurana, "Learning to swim in a sea of genomic data," *Genome Biology*, vol. 14, no. 12, p. 315, 2013.
- [21] H. T. Nguyen and L. T. Nguyen, "Fingerprints classification through image analysis and machine learning method," *Algorithms*, vol. 12, no. 11, pp. 1–11, 2019.
- [22] J. Sang, H. Wang, Q. Qian, H. Wu, and Y. Chen, "An efficient fingerprint identification algorithm based on minutiae and invariant moment," *Personal and Ubiquitous Computing*, vol. 22, no. 1, pp. 71–80, 2018.
- [23] M. M. H. Ali, V. H. Mahale, P. Yannawar, and A. T. Gaikwad, "Fingerprint recognition for person identification and verification based on minutiae matching," in *Proceedings-6th International Advanced Computing Conference, IACC*, pp. 332–339, Bhimavaram, India, February 2016.